Manuscript prepared for Clim. Past
with version 2014/09/16 7.15 Copernicus papers of the LaTeX class copernicus.cls.
Date: 6 December 2015

Phase relationships between orbital forcing and the composition of air trapped in Antarctic ice cores

Lucie Bazin[1], Amaelle Landais[1], Valérie Masson-Delmotte[1], Catherine Ritz[2], Ghislain Picard[2], Emilie Capron[3], Jean Jouzel[1], Marie Dumont[4], Markus Leuenberger[5], and Frédéric Prié[1]

[1]Laboratoire des Sciences du Climat et de l'Environnement, UMR8212, CEA–CNRS–UVSQ,Orme des Merisiers, Gif sur Yvette, France
[2]Laboratoire de Glaciologie et Géophysique de l'Environnement, UMR 5183, Univ. Grenoble Alpes–CNRS, Grenoble, France
[3]British Antarctic Survey, NERC, Cambridge, UK
[4]Météo–France–CNRS, CNRM–GAME UMR 3589, CEN, Grenoble, France
[5]Climate and Environmental Physics, Physics Institute and Oeschger Center for Climate Change Research, University of Bern, Bern, Switzerland

Correspondence to: Lucie Bazin (lucie.bazin@lsce.ipsl.fr)

Abstract. Orbital tuning is central for ice core chronologies beyond annual layer counting, available back to 60 ka (i.e. thousand of years before 1950) for Greenland ice cores. While several complementary orbital tuning tools have recently been developed using $\delta^{18}\mathrm{O}_{\mathrm{atm}}$, $\delta\mathrm{O}_2/\mathrm{N}_2$ and air content with different orbital targets, quantifying their uncertainties remains a challenge. Indeed, the exact processes linking variations of these parameters, measured in the air trapped in ice, to their orbital targets are not yet fully understood. Here, we provide new series of $\delta\mathrm{O}_2/\mathrm{N}_2$ and $\delta^{18}\mathrm{O}_{\mathrm{atm}}$ data encompassing Marine Isotopic Stage (MIS) 5 (between 100–160 ka) and the oldest part (340–800 ka) of the East Antarctic EPICA Dome C (EDC) ice core. For the first time, the measurements over MIS 5 allow an inter–comparison of $\delta\mathrm{O}_2/\mathrm{N}_2$ and $\delta^{18}\mathrm{O}_{\mathrm{atm}}$ records from three East Antarctic ice core sites (EDC, Vostok and Dome F). This comparison highlights a site–specific relationship between $\delta\mathrm{O}_2/\mathrm{N}_2$ and the water isotopic composition. Such a relationship and the difficulty to identify extrema and mid–slopes variations in $\delta\mathrm{O}_2/\mathrm{N}_2$ increase the uncertainty associated with the use of $\delta\mathrm{O}_2/\mathrm{N}_2$ as an orbital tuning tool, now calculated to be 3-4 ka. When combining records of $\delta^{18}\mathrm{O}_{\mathrm{atm}}$ and $\delta\mathrm{O}_2/\mathrm{N}_2$ from Vostok and EDC, we evidence a loss of orbital signature for these two parameters during periods of minimum eccentricity (∼400 ka, ∼720-800 ka). Our dataset reveals a time–varying offset between $\delta\mathrm{O}_2/\mathrm{N}_2$ and $\delta^{18}\mathrm{O}_{\mathrm{atm}}$ records over the last 800 ka that we interpret as variations in the lagged response of $\delta^{18}\mathrm{O}_{\mathrm{atm}}$ to precession. Larger offsets are identified during Terminations II, MIS 8 and MIS 16, corresponding to periods of destabilization of the Northern polar ice sheets. We therefore suggest that the occurrence of Heinrich–like events influences the response of $\delta^{18}\mathrm{O}_{\mathrm{atm}}$ to precession.

1 Introduction

Past changes in climate and atmospheric composition are recorded in a variety of ice core proxies. The EPICA Dome C (EDC) ice core has provided the longest available records, and documented glacial–interglacial changes in atmospheric greenhouse gases concentrations (Spahni et al., 2005; Loulergue et al., 2008; Lüthi et al., 2008) and Antarctic temperature (Jouzel et al., 2007) back to 800 ka (thousands of years before present, present being AD 1950). Precise and coherent ice core chronologies are critical to establish the sequence of events and to understand these past changes. A specificity of ice core chronologies lies in the requirement to calculate ice and gas chronologies, due to the fact that air is trapped several tens of meters below the ice sheet surface. This trapping process occurs at the so-called lock–in depth (LID).

Ice core age scales are usually constructed using ice flow models and different age constraints (Parrenin et al., 2001, 2004, 2007; Buiron et al., 2011). Lemieux-Dudon et al. (2010) have developed a new dating tool (Datice) allowing for the first time to produce an optimized and common chronology for several ice cores from Antarctica and Greenland, over the past 50 ka. Using an improved version of this dating tool, as well as an extended set of age constraints, Bazin et al. (2013) and Veres et al. (2013) have established a common chronology (AICC2012 chronology) for four Antarctic ice cores (Vostok; EDC; EPICA Dronning Maud Land, EDML; Talos Dome ice core, TALDICE) and one Greenland ice core (NorthGRIP, NGRIP) extending back to 800 ka for EDC. The construction of this chronology has been confirmed by an alternative bayesian tool, IceChrono (Parrenin et al., 2015). A key limitation in deep ice core chronologies lies in the lack of absolute age constraints prior to layer counting in NGRIP (for ages older than 60 ka, Svensson et al., 2008). Orbital tuning of several parameters measured in the air trapped in ice cores (air content, $\delta O_2/N_2$ and $\delta^{18}O_{atm}$) has thus played a central role for the construction of the AICC2012 chronology. Orbital tuning permits to attribute ages deduced from the integrated summer insolation, summer insolation or precession variations to their observed counterparts in air content, $\delta O_2/N_2$ or $\delta^{18}O_{atm}$ respectively, with acceptable uncertainties.

Orbital tuning is commonly applied to deep sea cores, using the orbital properties of benthic foraminifera $\delta^{18}O$ records, themselves related to changes in ice volume (Imbrie and Imbrie, 1980). The most closely related ice core parameter is $\delta^{18}O_{atm}$, $\delta^{18}O$ of atmospheric O_2. Ice core records of $\delta^{18}O_{atm}$ are strongly correlated with variations of insolation in the precession band, with a lag assumed to be $\sim$5–6 ka as established for the last termination (glacial–interglacial transition, Bender et al., 1994; Jouzel et al., 1996; Petit et al., 1999; Shackleton et al., 2000; Dreyfus et al., 2007). The modulation of precession on $\delta^{18}O_{atm}$ operates through the biosphere productivity and changes in low latitude water cycle (Bender et al., 1994; Malaizé et al., 1999; Wang et al., 2008; Severinghaus et al., 2009; Landais et al., 2007, 2010). The significant time delay between precession and $\delta^{18}O_{atm}$ is not straightforward to explain. It partly depends on the 1–2 ka residence time of O_2 in the atmosphere and on the complex response of biosphere productivity and tropical water cycle to precession changes. Caley et al. (2011) have shown lags of several thousand years between the responses of Indian and Asian monsoon systems to orbital forcing over the last 40 ka. Moreover, variations of $\delta^{18}O_{atm}$ are not only affected by the response to orbital forcing, but also by the millennial climate variability (Severinghaus et al., 2009; Landais et al., 2007). During Terminations I and II, $\delta^{18}O_{atm}$ maxima have been linked to Heinrich stadials 1 and 11 (Landais et al., 2013). Because of these complex interactions, the lag between $\delta^{18}O_{atm}$ and precession should vary with time (Leuenberger, 1997; Jouzel et al., 2002). However, for dating purposes, this lag has been assumed to be constant with an uncertainty of a quarter of a precession cycle (6 ka ; Parrenin et al., 2007; Dreyfus et al., 2007).

Associated with a completely different underlying mechanism, two other ice core parameters have also been used for orbital tuning. The air content and $\delta O_2/N_2$ measured in the air trapped in ice cores are controlled by the enclosure process near the close-off depth (depth of closure of ice interstices and formation of air bubbles). At this depth, a depletion of the ratio O_2/N_2 compared to the atmospheric ratio is observed and attributed to the smaller size of O_2 molecules compared to N_2 ones (Battle et al., 1996; Huber et al., 2006; Severinghaus and Battle, 2006). It is expected that the entrapment process and the associated O_2 effusion or permeation effects are linked to the physical properties of snow at this depth. Because snow metamorphism is very strong at the surface of the ice sheet in summer (Town et al., 2008; Picard et al., 2012), snow physical properties are expected to be driven by local summer insolation. Records of $\delta O_2/N_2$ and air content measured at Vostok, Dome F and EDC indeed depict variability at orbital frequencies, which appear in phase with local summer insolation (Bender, 2002; Kawamura et al., 2007; Raynaud et al., 2007; Lipenkov et al., 2011; Landais et al., 2012).

In summary, $\delta^{18}O_{atm}$ provides a relationship between the gas phase age and orbital forcing, due to changes in atmospheric composition driven by changes in low latitude hydrological cycle and biosphere productivity. Air content and $\delta O_2/N_2$ provide a relationship between the ice phase age and local insolation, due to the impact of snow metamorphism on air trapping processes.

$\delta^{18}O_{atm}$ is a well–mixed atmospheric signal, allowing synchronization of different ice core records. It also has the potential to link ice cores with climate records from other latitudes (e.g. global ice volume, low latitude hydrological cycle and biosphere productivity). However, due to the numerous and complex processes affecting the $\delta^{18}O_{atm}$, this orbital dating tool is generally associated with an uncertainty of 6 ka. An important challenge to progress on chronological issues is to estimate the variations of the lag between $\delta^{18}O_{atm}$ and precession over the last eight glacial–interglacial cycles.

Contrary to $\delta^{18}O_{atm}$, $\delta O_2/N_2$ and air content are not influenced by remote climatic–driven signals such as low latitude hydrological cycle or northern hemisphere land ice volume. Fujita et al. (2009) proposed a model to explain both total air content (effusion effect) and $\delta O_2/N_2$ (permeation effect) variations. This model is based on the different densification rates of layers affected by strong surface metamorphism and layers affected by low surface metamorphism. It is known that the snow metamorphism near the surface is the most rapid and strongest owing to the higher temperature (in summer) and high temperature gradient (Libois et al., 2014). Thus even if the residence time of the snow in the near-surface layer (e.g. 10 cm depth) is very small compared to the time required to reach the close–off depth, the metamorphism occurring during this short period results in major micro-structural changes in the snow. The near-surface metamorphism can be at least partially preserved down to the close-off depth. It is therefore expected that all factors integrated in the surface snow energy budget (air temperature, snow albedo, solar radiation penetration depth), controlling the temperature profil in snow, have an impact on snow metamorphism (Picard et al., 2012). Moreover, strong modifications of layering and microstructure are also observed at several tenths of meters below the surface (Hörhold et al., 2012). It is therefore expected that pore structure at close-off is also affected by changes in dust load (Freitag et al., 2013). Finally, the direct effect of accumulation rates cannot be neglected in these processes (Hutterli et al., 2010). Accumulation rate will indeed have a direct influence on the permeation mechanism proposed by Fujita et al. (2009) through the increase of the pressure difference between open and closed bubbles near the close-off and the increase of the depth of the non-diffusive zone at the bottom of the firn (Witrant et al., 2012). The direct link classically assumed between summer solstice insolation and $\delta O_2/N_2$ variations is therefore complicated by these different influences. Suwa and Bender (2008a) have observed a very different $\delta O_2/N_2$ vs summer solstice insolation relationship for the high accumulation rate site of GISP2 in Greenland compared to the low accumulation rate sites of the East Antarctic plateau.

These different limitations for each parameter have recently motivated a first assessment of the coherency between the different orbital dating tools in ice cores. Indeed, in the framework of the AICC2012 chronology construction (Bazin et al., 2013), we took advantage of available records of $\delta O_2/N_2$, air content and $\delta^{18}O_{atm}$ over the period 100–400 ka of the Vostok ice core (Petit et al., 1999; Bender, 2002; Suwa and Bender, 2008b; Lipenkov et al., 2011). We showed that the final chronology was the same using one or the other orbital markers with uncertainties of up to 7 ka, 4 ka and 6 ka for air content, $\delta O_2/N_2$ and $\delta^{18}O_{atm}$, respectively. However, this first assessment was restricted to one single ice core covering only the last 400 ka. The large uncertainties associated with the different orbital age markers in this case were partly due to the low resolution of the existing records and to the poor quality of the $\delta O_2/N_2$ data affected by gas loss (Landais et al., 2012). Gas loss, which occurs through micro–cracks during coring and ice core storage at warm temperature (typically freezers at -25°C), favours the loss of O_2, and alters the original $\delta O_2/N_2$ signal (Kawamura et al., 2007; Bender et al., 1995). In that case, drifts in $\delta O_2/N_2$ have been shown to be related to storage duration (Kawamura et al., 2007) and must be corrected prior to the use of the data.

Our current understanding of these dating tools motivates further comparison of $\delta O_2/N_2$ and $\delta^{18}O_{atm}$ records, obtained (i) at high temporal resolution, (ii) from different East Antarctic ice cores, (iii) under different orbital and climatic contexts and (iv) on ice stored at very cold temperature (-50°C) to avoid gas loss correction. In order to complement existing records from the Vostok and

Dome F ice cores, we have performed new measurements on the long EDC ice core, for which only parts of the $\delta O_2/N_2$ record were obtained from samples of well–conserved ice (-50°C) (Landais et al., 2012).

For this purpose, we have performed new measurements of $\delta^{18}O_{atm}$ and $\delta O_2/N_2$ on ice stored at -50°C (i.e. non-affected by gas loss) on the EDC ice core over Marine Isotope Stage (MIS) 5 and between 340–800 ka. Section 2 describes the new measurements from the EDC ice core complementing previous data (Dreyfus et al., 2007, 2008; Landais et al., 2012; Bazin et al., 2013; Landais et al., 2013). Section 3 is dedicated to the analyses of the datasets, the inter–comparison of Vostok, Dome F and EDC data over MIS 5, as well as an investigation of the time offsets between $\delta O_2/N_2$ and $\delta^{18}O_{atm}$ during the past 800 ka and their implications for orbital tuning. These records enable us to check the coherency of these parameters for orbital tuning and to provide recommendations for their use in ice core chronologies.

2 Analytical method and measurements

The measurements of the isotopic composition of air trapped in well–conserved ice from EDC were performed at LSCE. The samples were cut in Antarctica in the archive trench at -40°C maximum, and then kept at -50°C during transportation and storage. Measurements were performed only a few months after their transportation from Antarctica. To prevent any contamination from exchanges with ambient air due to micro–cracks, we shave off 3–5 mm of ice on each face, and the air is extracted from a sample of ~10 g of ice. Two different extraction methods have been used, either a manual or a semi–automatic line.

The manual method consists of a melt–refreeze technique (Sowers et al., 1989; Landais et al., 2003) for extracting the air trapped in the ice samples. The sample is placed in a cold flask and then the air in the flask is pumped. The trapped air is extracted by melting and refreezing the sample and is then cryogenically transferred in a stainless–steel tube immersed in liquid helium.

For the semi–automatic extraction line, we proceed with two exterior air samples and three ice samples with duplicates each day. The samples are placed in cold flasks and the air in the flasks is pumped; the air trapped in ice is extracted by melting of the samples and left at room temperature during one hour minimum. The air samples are then transferred one at a time through CO_2 and water vapour traps before being cryogenically trapped into a manifold immersed in liquid helium. An inter–comparison of the two extraction lines has been conducted using air extracted from NGRIP ice samples. No bias is observed in–between the two analytical extraction methods.

After a waiting time of 40 min, allowing the tubes to reach room temperature, measurements are performed with a dual inlet Delta V plus (Thermo Electron Corporation) mass spectrometer. A classical run is composed of 16 measurements of the sample in parallel with 16 measurements of a standard of dried exterior air. We simultaneously measure $\delta^{18}O$, $\delta O_2/N_2$ and $\delta^{15}N$. The data are then calibrated against the mean exterior air values and corrected for mass interferences following the standard methodologies (Severinghaus et al., 2001; Landais et al., 2003).

We were able to replicate 152 samples over 189 depth levels due to the small size of samples. The $\delta O_2/N_2$ and ^{18}O measurements are corrected for gravitational fractionation using the following equations:

$$\delta^{18}O_{atm} = \delta^{18}O - 2 \cdot \delta^{15}N \quad (1)$$

$$\delta O_2/N_2 = \delta O_2/N_{2_{raw}} - 4 \cdot \delta^{15}N \quad (2)$$

The final precision (pooled standard deviation) for our new set of data is 0.02 ‰ for $\delta^{18}O_{atm}$ and 0.77 ‰ for $\delta O_2/N_2$.

3 Results and discussion

Figure 1 shows the full EDC $\delta^{18}O_{atm}$ dataset, which has a mean temporal resolution of 1.1 ka thanks to our new data completing the records of Dreyfus et al. (2007, 2008), Bazin et al. (2013) between 300–800 ka and Landais et al. (2013) over MIS 5. The data depict variations that coincide with those of precession, together with larger changes associated with glacial terminations. The good overall agreement between variations in precession and the signal in $\delta^{18}O_{atm}$ only breaks during periods of low eccentricity: between 350 and 450 ka (MIS12–11–10) and around 700 to 800 ka. As already observed by Dreyfus et al. (2007), our new results illustrate that precession–driven variations in $\delta^{18}O_{atm}$ are reduced during these periods of low eccentricity. Moreover, with the addition of our new data, the tuning performed by Dreyfus et al. (2007) between 530–550 ka is not as straightforward as previously presented. Still, this stays within the uncertainties associated with $\delta^{18}O_{atm}$ orbital tuning and has no impact on the chronology construction.

Spectral analyses of the $\delta^{18}O_{atm}$ record spanning 300–800 ka (Figure 2) confirm earlier results obtained by Dreyfus et al. (2007) for EDC, and those obtained for Vostok and Dome F data over the last 400 ka (Petit et al., 1999; Kawamura et al., 2007). The major peaks are observed for periods of 100 ka, 19–23 ka, and 41 ka (by decreasing amplitude) and correspond respectively to the eccentricity and/or glacial–interglacial climatic variations, precession and obliquity bands.

Our new data allow us to establish a record of $\delta O_2/N_2$ covering MIS 5 and between 340–800 ka measured on well–conserved ice (Figure 1). Series A (392–473 ka) and B (706–800 ka) were measured in 2007–2008 (Landais et al., 2012) and are complemented by our new set of data (Series C). The mean temporal resolution of the complete $\delta O_2/N_2$ record is 2.37 ka over MIS 5 and 2.08 ka between 340–800 ka. The pooled standard deviations of each dataset vary between 0.3 and 1 ‰ (A: 0.32 ‰, B: 1.03 ‰; C: 0.77 ‰).

When compared with earlier data affected by gas loss (Landais et al., 2012), our data show the same timing of variations of $\delta O_2/N_2$ that coincide with those of local summer solstice insolation at Dome C (Appendix A). However, the relative strengths of minima and maxima of $\delta O_2/N_2$ do not scale with those of summer insolation. Large amplitudes of summer insolation cycles are associated with relatively small amplitudes of the corresponding cycles in $\delta O_2/N_2$ and vice versa (Figure 1) and only 13% of the variance of the raw $\delta O_2/N_2$ data is explained by summer solstice insolation. Finally, the new record reveals an overall decreasing trend of $\delta O_2/N_2$ over the last 800 ka at EDC (0.79 ± 0.08 ‰/100 ka), confirming the observations of Landais et al. (2012) on their composite curve (Appendix A). Moreover, this feature was already identified during the last 400 ka at Vostok (0.56 ± 0.33 ‰/100 ka) and 360 ka at Dome F (0.56 ± 0.28 ‰/100 ka). We conclude that the long term decreasing trend of $\delta O_2/N_2$ with time is not an artifact due to the gas loss correction, but it may still be linked with a different preservation of the air with varying depth in the ice core. Long term changes in the enclosing process or modification in the atmospheric ratio O_2/N_2 can also be evoked.

The spectral analysis of the new EDC $\delta O_2/N_2$ record between 340–800 ka (Figure 2) depicts peaks associated with the precession and obliquity bands (19–23 ka and 41 ka), together with a 100 ka periodicity. This 100 ka period was neither observed in $\delta O_2/N_2$ records from other Antarctic ice cores (Bender, 2002; Kawamura et al., 2007) nor in the composite EDC record of Landais et al. (2012).

The 100 ka peak is also absent from the power spectrum of summer solstice insolation, independently of the time window considered (Figure 2). The 100 ka signal in $\delta O_2/N_2$, most strongly imprinted between 500 and 700 ka, arises from pronounced minima in the $\delta O_2/N_2$ record at 450, 550 and 650 ka. These minima occur during glacial periods characterized by low eccentricity, and therefore coincide with local insolation minima (Figure 1). The 100 ka periodicity identified in the EDC $\delta O_2/N_2$ record between 340–800 ka, and absent from records spanning 0–400 ka may thus arise from a reduced influence of precession–driven insolation changes on snow metamorphism during eccentricity minima, similarly to the reduced precession–driven signal in $\delta^{18}O_{atm}$. The weakening of insolation influence would leave room for other factors to impact EDC $\delta O_2/N_2$ such as local climatic parameters. Indeed, records of local climate (e.g. water stable isotopes and inferred changes in local temperature and accumulation rate, dust) exhibit a strong peak at 100 ka, characteristic of glacial–interglacial cycles (Figure 2, Masson-Delmotte et al., 2010; Lambert et al., 2008).

3.1 MIS 5 Antarctic inter–comparison

Our EDC $\delta O_2/N_2$ record displays variability in the precession and obliquity ranges, as well as minima and maxima that highlight clear similarities with local summer insolation. However, neither the modulation in amplitude nor the 100 ka signal are related to local summer insolation, pointing to other local parameters affecting the snow metamorphism and firnification processes. Potential candidates that may imprint on $\delta O_2/N_2$ with a 100 ka period would be changes in temperature, accumulation rate, firn dust content or component of the surface energy budget. While variations in summer solstice insolation are expected to be very similar in all East Antarctic ice core drilling sites, differences in site characteristics (e.g. snow properties, meteorological situation, mean climate) may cause differences in the $\delta O_2/N_2$ signals from different ice cores. This motivates a comparison of $\delta O_2/N_2$ signals from three ice cores drilled in the East Antarctic plateau: Dome F, Vostok and EDC. Present–day conditions at these three dry and particularly cold sites depict differences in the distance to open ocean, elevation (within 577 m), albedo (within 3%), wind speed (a factor of two), accumulation (within 15%) and mean annual temperature (within 2.5°C) (Table 1).

Thanks to our new $\delta O_2/N_2$ data, we now have records of both $\delta O_2/N_2$, $\delta^{18}O_{atm}$ and water stable isotopes over MIS 5 from EDC, Dome F and Vostok. MIS 5 is characterized by large precession parameter variations, together with large glacial-interglacial changes in Antarctic temperature, and present warmer–than–present reconstructed interglacial temperatures (Sime et al., 2009; Stenni et al., 2010; Masson-Delmotte et al., 2011; Uemura et al., 2012).

Figure 3 displays the $\delta O_2/N_2$ records from Dome F (on the DFO-2006 time scale, Kawamura et al., 2007), EDC and Vostok (both on their respective AICC2012 chronologies, Veres et al., 2013; Bazin et al., 2013) from 150 to 100 ka. We observe the same orbital scale variations from all three records, i.e. a $\delta O_2/N_2$ maximum at around 126 ka bracketed by 2 minima at 115 and 135 ka. Two major differences are still noticeable:

- a lower $\delta O_2/N_2$ mean value and greater amplitude in variations at Vostok than at Dome F and EDC.
- a site–specific high frequency variability. For instance, between 100 and 115 ka, EDC and Vostok $\delta O_2/N_2$ records show a double peak that is not observed at Dome F and significantly larger than measurements uncertainties.

The gas loss corrections applied on the Dome F and Vostok $\delta O_2/N_2$ records may explain part of these discrepancies. The resolution of the records (2.3 ka for EDC, 1.5 ka for Vostok and 1.2 ka for Dome F between 100-150 ka) limits the comparison of high frequency variations observed between 100 and 115 ka and around 126 ka. In the Greenland GISP2 ice core, it has been shown that $\delta O_2/N_2$ can display millennial scale variability, in relationship with glacial climatic variability (Suwa and Bender, 2008a). Only high-resolution measurements conducted on well–conserved ice could allow us to have an objective discussion of high frequency signals in Antarctic ice.

EDC, Vostok and Dome F $\delta O_2/N_2$ records present variations that occur simultaneously with the ones of the local summer solstice insolation target curves (Figure 3). This is expected since the different ice core chronologies used in Figure 3 are based at least partially on the alignment of the $\delta O_2/N_2$ signal on the summer solstice insolation curve. The identification of the $\delta O_2/N_2$ extrema and mid-slopes within the three records indicates that the $\delta O_2/N_2$ variations can be considered synchronous, within the calculated uncertainty, for the three sites over this period (Appendix B). This method of identification, taking into account the scattering of the data, the resolution and the chronology uncertainty, gives an error of 3-4 ka for this orbital tuning method for EDC, Vostok and Dome F (Appendix B).

An intriguing feature arises from the comparison of the relative lags between the $\delta O_2/N_2$, $\delta^{18}O_{atm}$ and $\delta^{18}O_{ice}$ records within each ice core (Figure 3). While the $\delta O_2/N_2$ records of the three sites seem aligned, Dome F $\delta^{18}O_{atm}$ and $\delta^{18}O_{ice}$ exhibit a fingerprint of Termination II occurring 2 ka earlier than the ones recorded in Vostok and EDC (as observed on water stable isotope optima, Figure 3 and Bazin et al. (2013)). A larger offset (up to 6 ka) is even observed for the glacial inception between Dome F and EDC/Vostok $\delta^{18}O_{atm}$ and $\delta^{18}O_{ice}$ records. This particular feature is persistent after volcanic synchronization between EDC and Dome F ice cores (Appendix C; Fujita et al., 2015). In Fujita et al. (2015), potential causes for this large age offset between the DFO-2006 and AICC2012 chronologies are suggested to come from an overestimation of the surface mass balance in the glaciological approach and/or an error in one of the $\delta O_2/N_2$ age constraint by 3ka. In this study, as the transfer from one chronology to the other (either DFO-2006 on AICC2012 or the other way around) do not improve significantly the correlation between the $\delta O_2/N_2$ records of EDC and Dome F (Appendix C), we suggest that this behaviour over the glacial inception results from different relationships between $\delta O_2/N_2$ and the water stable isotopes at these two sites.

Our results from the MIS 5 comparison and the significant 100 ka period observed in the spectral analysis of $\delta O_2/N_2$ support the influence of local climatic parameters on $\delta O_2/N_2$ variations. In addition, the influence of climatic and environmental parameters differences between sites may also result from a different response of snow metamorphism and therefore $\delta O_2/N_2$ to orbital forcing.

First, we investigate how changes in layering or snow microstructure during the firnification processes can affect $\delta O_2/N_2$. Several indices indeed suggest that $\delta O_2/N_2$ is not only influenced by the energy received at the surface of snow but also by firnification processes, which themselves depend on climatic conditions such as accumulation rate, firn temperature, impurity content of the snow (Hutterli et al., 2010). We have thus searched for local climatic influence on $\delta O_2/N_2$ focusing first on accumulation rates. No significant correlation can be identified between EDC accumulation rate produced by AICC2012 and $\delta O_2/N_2$ variations (R= 0.107 between 340–800 ka). Kobashi et al. (2015) observe a significant correlation between the $\delta Ar/N_2$ on the gas age and the accumulation rate for Greenland ice cores over the Holocene. Following their observation, we have calculated the correlation between our $\delta O_2/N_2$ record and the corresponding accumulation rate at the age corrected of the delta–age (equivalent to the gas age). No significant correlation is identified (R=0.134 between 340–800 ka). The absence of significant correlation between the $\delta O_2/N_2$ record and accumulation rate probably reflects a non straightforward relationship between these two quantities. In particular, the relationship between $\delta O_2/N_2$ and accumulation rate appears to be more complicated for low accumulation rate sites at orbital timescale than in Greenland over the Holocene.

Second, changes in dust concentration have been suggested to potentially influence firn density and hence air trapping (Hörhold et al., 2012; Freitag et al., 2013). Records of dust concentration spanning MIS 5 are available for EDC (Lambert et al., 2008) and Vostok (Petit et al., 1999). There is no significant difference between the dust concentration of Vostok and EDC regarding their amplitude and timing of changes, so they should have the same effect at both sites. The lack of published $\delta O_2/N_2$ and dust records from Dome F precludes investigations of the differences between Dome F and Vostok–EDC. Moreover, subsurface processes and reworking of surface snow by the wind are known to have an influence on actual firnification, as a result this should have an impact on the $\delta O_2/N_2$ trapping process (Fujita et al., 2012), even under glacial climatic conditions.

Third, we explore if inter–site differences in surface albedo could explain differences in the energy input for surface snow metamorphism (Picard et al., 2012). Surface albedo is currently measured over East Antarctica with MODIS multispectral imager on board TERRA and AQUA satellites. Data collected since 2001 enable to compare the albedo of our three sites of interest (Table 1). For this purpose, White Sky broadband albedo data (surface albedo under perfectly diffuse illumination conditions) were extracted from MCD43A3 products (http://www.umb.edu/spectralmass/terra_aqua_modis/v006). Only values for which local solar noon sun zenith angle is less than 65° and high quality flags (QA=0 in MCD43A2 products) are considered (Schaaf et al., 2011). They show similar values at Vostok and EDC (0.83), and significantly lower values at Dome F (0.80). This implies that, today, about 15% more incoming solar radiations are absorbed by Dome F surface snow and can act on its metamorphism. However, surface metamorphism is not simply related to surface albedo. This can be investigated using the grain index time series developed by Picard et al. (2012). The amplitude of diurnal cycles and grain size near the surface indicate more metamorphism at Dome C than at Dome F. We note that the largest amplitude of grain growth is observed at South Pole, despite a high local albedo and no diurnal cycle. While present day data provide a hint for possible differences in surface snow metamorphism, further studies are needed to better understand how the surface energy budget controls the surface and subsurface snow metamorphism, and how it can explain the differences in $\delta O_2/N_2$ mean level and phasing between $\delta O_2/N_2$ and insolation forcing at different sites.

Finally, one important assumption for the process linking $\delta O_2/N_2$ and orbital forcing is that snow metamorphism is maximum at peak temperature (Kawamura et al., 2007) so that summer solstice insolation curve should be taken as orbital target for $\delta O_2/N_2$ variations. At Dome F, the current seasonal cycle of surface snow temperature measurements shows maximum values at the summer solstice (21 December, Kawamura et al., 2007). At Vostok, the maximum of surface snow temperature is observed about 10 days later, close to December 30$^{\text{th}}$ (continuous measurements since 2010, Lefebvre et al. (2012), J.-R. Petit pers. comm.). At Dome C, three years continuous measurements of surface snow temperature between 2006–2009 have shown that the maximum of temperature occurs 15–20 days after the summer solstice (Landais et al., 2012, confirmed by the continuous measurements since then). These regional differences highlight the fact that, today, surface snow temperature does not reach its summer maximum in phase with local summer solstice insolation. As a consequence, different insolation target curves for $\delta O_2/N_2$ should be considered for the different sites if the observations performed for present day conditions are also valid for the past. Following this observation, we have tried to use December 30$^{\mathrm{th}}$ and January 15$^{\mathrm{th}}$ insolation curves as respective orbital targets for EDC and Vostok $\delta O_2/N_2$ records. However, using such orbital targets strengthens the lag between the Dome F and Vostok–EDC age scales over MIS 5.

This study provides support for more complex processes affecting the $\delta O_2/N_2$ than just the local summer solstice modulation. We cannot yet explain the origin of such site specific behaviour of $\delta O_2/N_2$ as we are limited by the lack of available data ($\delta O_2/N_2$ on well–conserved ice for Vostok and Dome F, dust records for Dome F, CH_4 for Dome F, coherent chronology for all three sites) and by our current understanding of firnification processes. However, from the available information we can point to a cautious use of orbital age markers inferred from $\delta O_2/N_2$ with possible differences from one site to another. Based on the inter–site differences, we recommend to use an uncertainty of 3–4 ka, and to combine these data with other dating tools.

3.2 $\delta O_2/N_2$ – $\delta^{18}O_{atm}$ offset

A lag of $\delta^{18}O_{\mathrm{atm}}$ vs precession was observed over the last termination at Vostok, EDC and GISP2 with values of 5.8 ka, 5.9 ka and 5.3 ka on the FGT1, EDC3 and Meese/Sowers chronologies respectively (Dreyfus et al., 2007; Petit et al., 1999; Parrenin et al., 2004, 2007; Bender et al., 1994; Meese et al., 1994). On the new AICC2012 chronology, the lag of $\delta^{18}O_{\mathrm{atm}}$ with precession over Termination I is now of 5.6 ka for Vostok and 5.5 ka for EDC.

During Termination II, recently published high–resolution $\delta^{18}O_{\mathrm{atm}}$ measurements (Landais et al., 2013) together with the AICC2012 chronology (Bazin et al., 2013) also give a $\sim$5 ka phase lag (5.2 ka) between precession and $\delta^{18}O_{\mathrm{atm}}$. Bazin et al. (2013) have shown an excellent agreement for the timing of Termination II on a purely orbital ice core chronology (AICC2012 using only ice core orbital age markers over Termination II) and an independent speleothem chronology based on U/Th Dating (Cheng et al., 2009). This comparison rely on the assumption that abrupt variations in CH_4 and calcite $\delta^{18}O$ are synchronous. While this assumption was explicitly used to build the EDC3 chronology (Parrenin et al., 2007; Waelbroeck et al., 2008), this is not the case for AICC2012, which provides high confidence in the accuracy of this chronology for Termination II.

The determination of the lag between $\delta^{18}O_{\mathrm{atm}}$ and precession for earlier terminations is more complicated. Indeed, it requires an absolute chronology that is independent from orbital tuning based on $\delta^{18}O_{\mathrm{atm}}$. Similarly, determining the phase lag between $\delta O_2/N_2$ and summer solstice insolation is not possible in the absence of an alternative timescale free from $\delta O_2/N_2$ constraints. However, we can still progress on the issue of relative offsets between $\delta^{18}O_{\mathrm{atm}}$, $\delta O_2/N_2$ and orbital targets by studying the relationships between $\delta O_2/N_2$ and $\delta^{18}O_{\mathrm{atm}}$. Indeed, even if the orbital targets of both parameters are close and without significant lags between them (less than 500 years over the last 800 ka), $\delta^{18}O_{\mathrm{atm}}$ and $\delta O_2/N_2$ variations are induced by very different mechanisms (remote for

$\delta^{18}O_{atm}$, local for $\delta O_2/N_2$). As a consequence, it is very unlikely that lags or leads of $\delta^{18}O_{atm}$ and $\delta O_2/N_2$ relative to their orbital targets would occur simultaneously. These changes should then be visible on the lead and lag between $\delta O_2/N_2$ and $\delta^{18}O_{atm}$.

Based on the good agreement of the Vostok and EDC $\delta O_2/N_2$ records over MIS 5, we combine the full Vostok (0–400 ka) and EDC (340–800 ka) $\delta O_2/N_2$ and $\delta^{18}O_{atm}$ records (Figure 4). We re-interpolate the data according to the largest sampling resolution between the $\delta O_2/N_2$ and $\delta^{18}O_{atm}$ records of each sites (2.07 ka for EDC and 1.76 ka for Vostok). There is a close resemblance of the interpolated and original data. In order to calculate the relative offset between the two proxy records, we normalize the data (minus the mean, divided by the standard deviation) and filter them between 15–100 ka using wavelet transform. The filter is computed using Fourier transform and convolution products. The delay is deduced through the conversion of the phase calculated between the $\delta O_2/N_2$ and $\delta^{18}O_{atm}$ filtered records after cross-correlation. An independent estimation of the offset has been manually calculated from the identification of the timing of extrema in both records following the same methodology as in Appendix B.

During periods of weak eccentricity (e.g. around 400 ka and before 720 ka), there is no clear correspondence between the variations of $\delta O_2/N_2$ and $\delta^{18}O_{atm}$ compared to the variations of their orbital target curves, as previously noted (Dreyfus et al., 2007; Landais et al., 2012). During these periods, the variations of insolation in the precession band are probably too small to be imprinted in either $\delta O_2/N_2$ or $\delta^{18}O_{atm}$ records. We choose to disregard the EDC $\delta^{18}O_{atm}$–$\delta O_2/N_2$ offsets before 550 ka because the $\delta O_2/N_2$ record do not resemble the insolation variations over MIS 13 (Figure 1). Finally, the most recent 100 ka correspond to a period of low eccentricity and the $\delta O_2/N_2$ signal does not display any variability comparable to the insolation curve one (before the air bubbles/clathrates transition). As a consequence, we disregard these periods for our discussion of the phase delay (not shown on Figure 4). This also means that the orbital tuning through $\delta^{18}O_{atm}$ and $\delta O_2/N_2$ is much less reliable over these periods. We therefore recommend excluding such orbital tie points during large eccentricity minima, or considering them with larger uncertainties for dating purposes. The time intervals covered by the following discussion correspond to 100–350 ka (Vostok data) and 550–720 ka (EDC data).

During the remaining intervals of intermediate to strong eccentricity, the offset between $\delta O_2/N_2$ and $\delta^{18}O_{atm}$ varies between -6 and -1 ka in the Matlab delay and between -8 +1 ka for the manually calculated one (Figure 4). The Matlab-based calculated delay tends to present smoother and less marked variations than the manual one. Both estimations are generally in agreement regarding the calculated uncertainty. For Termination II, we obtain a $\delta^{18}O_{atm}$ vs $\delta O_2/N_2$ phase delay of 4.5 ka, which is in good agreement with the $\delta^{18}O_{atm}$ vs precession lag observed on raw data and a zero phase between $\delta O_2/N_2$ and summer solstice insolation as displayed on Figure 3. On Figure 4, we observe minimal offsets during MIS 6–7, the end of MIS 9, the end of MIS 14–start of MIS 15 and the end of MIS 17. These periods are marked by high eccentricity levels together with intermediate ice–sheet extents (i.e. neither full glacial conditions nor extremely warm interglacial conditions). On the contrary, local maxima of the $\delta O_2/N_2$–$\delta^{18}O_{atm}$ phase delay are observed for Termination II (-4.5 ka), MIS 8 (-5 ka) and MIS 16 (-3 ka). Over MIS 15, the offset calculated with Matlab tends to increase while the manually calculated one presents a larger variability.

Part of the variations in the offset value between $\delta O_2/N_2$ and $\delta^{18}O_{atm}$ may be due to the uncertainty in the age difference between ice and gas ages since $\delta^{18}O_{atm}$ is expressed on a gas timescale while $\delta O_2/N_2$ is on an ice timescale. Such uncertainty is largest during glacial periods, due to the impact of glacial climate conditions on firn processes. This uncertainty always stays below 1 ka, and therefore cannot explain the observed variations in delay value between $\delta O_2/N_2$ and $\delta^{18}O_{atm}$. We argue that the large variations of the lag observed between $\delta O_2/N_2$ and $\delta^{18}O_{atm}$ are mainly due to variations in the relationship between $\delta^{18}O_{atm}$ and precession, as $\delta O_2/N_2$ can be considered synchronous with local insolation and there is nearly no differences in timing of insolation and precession variations. Indeed, the link between precession and $\delta^{18}O_{atm}$ is not direct and involves global modifications of the low latitude water cycle and biosphere productivity. On the opposite, while the exact mechanism linking $\delta O_2/N_2$ to summer solstice insolation is not yet fully understood, there is no doubt that it involves local firn processes with a faster response time.

Many reasons are invoked to explain the phase lag between precession and $\delta^{18}O_{atm}$. As evidenced over Terminations I and II and over the last 240 ka, $\delta^{18}O_{atm}$ variations are closely related to the dynamic of the low latitude hydrological cycle (Wang et al., 2008; Severinghaus et al., 2009; Landais et al., 2007, 2010, 2013; Cheng et al., 2009). Monsoons are influenced by orbital forcing, with a strong imprint of precession (Wang et al., 2008; Braconnot et al., 2008), but also by the millennial scale variability (Wang et al., 2001; Marzin et al., 2013). The Heinrich event 1 is for instance associated with a weak monsoon interval (e.g. Denton et al., 2010). We note that Termination I and Termination II are associated with large Heinrich events during the first part of the deglaciation, when orbital forcing already acts on sea level and global climate, including Antarctic temperature (Landais et al., 2013). Severinghaus et al. (2009) have observed a systematic increase of $\delta^{18}O_{atm}$ during Heinrich events over the last glacial period, these events being imprinted both in the calcite $\delta^{18}O$ and ice core $\delta^{18}O_{atm}$. Following this finding, Reutenauer et al. (2015) used outputs from coupled climate model and atmospheric general circulation model equipped with water isotopes to estimate the change of $\delta^{18}O_{atm}$ induced by a freshwater input. These calculations show that the increase of $\delta^{18}O_{atm}$ during a Heinrich event is induced by a southward shift of the ITCZ associated with the freshwater input that leads to an increase of the $\delta^{18}O$ of the low latitude meteoric water in the northern hemisphere. This signal is then transmitted to the $\delta^{18}O$ of O_2 through photosynthesis of the important terrestrial biosphere in the low latitude Northern Hemisphere during the last glacial period. The occurrence of freshwater input can thus delay the change in $\delta^{18}O_{atm}$ induced by the sole insolation. This mechanism would satisfactorily explain lags of $\delta^{18}O_{atm}$ behind insolation when Heinrich events are observed.

In order to study the possible link between variations of the $\delta O_2/N_2$–$\delta^{18}O_{atm}$ offset and the occurrence of Heinrich events, we confront our results with marine records from cores U1302/03 and U1308 located within the IRD belt of North Atlantic (Figure 4 E, F, G Hodell et al., 2008; Channell et al., 2012; Channell and Hodell, 2013). Sites U1302/03 and U1308 are located on the western and eastern borders of the IRD belt respectively. Heinrich events consist in large iceberg discharges of the Laurentide ice sheet through the Hudson Strait. These events are well recorded by spikes in the Ca/Sr ratio, which traces the abundance of carbonate grain in the sediment. On the contrary, IRD events corresponding to discharges of the Greenland and/or European ice sheets (Fennoscandian, British ice sheets mainly) are identified by large amounts of detrital quartz in the sediment, then characterized by peaks in the Si/Sr ratio. Consequently, thanks to their respective locations, the Ca/Sr record of core U1302/03 is a good proxy for the Hudson Strait iceberg events (Heinrich-like events), and the Si/Sr record of core U1308 is a good representative for the Greenland/European ice sheets destabilization events. The marine cores data on Figure 4 are presented on their original chronologies, constructed by tuning of their $\delta^{18}O$ to the LR04 benthic stack (Lisiecki and Raymo, 2005). The uncertainty associated with this dating method is estimated to be 4 ka for the last 1 million years. Such a large uncertainty prevents us from any comparison of absolute timing of ice sheets discharge events with our ice core records. We thus only discuss the occurence of Heinrich-like events and Greenland/European ice sheets discharges in regards to the variation of the $\delta O_2/N_2$–$\delta^{18}O_{atm}$ offset..

We can see that major spikes in Ca/Sr and Si/Sr recorded in the marine cores occur at roughly the same periods as the maximum $\delta O_2/N_2$–$\delta^{18}O_{atm}$ offset values. The correspondance is especially well marked in the manually calculated offsets (red circles and arrows on Figure 4). The lag values over MIS 15 do not present the same variability in both offset estimates as previously noticed. In the marine records of iceberg discharge we only see small but regular peaks in the Ca/Sr record during this period. For Channell et al. (2012), these peaks do not reflect the occurence of Heinrich-like events but most probably correspond to debris flows or glacial-lake drainage events caused by changes in hydrological budget or changes in base level. Compared to our $\delta O_2/N_2$–$\delta^{18}O_{atm}$ offsets records, we suggest that the manually calculated delay may reflect these individual events while the Matlab delay may just integrate them all progressively due to the filtration of the data.

Interpreting the chosen marine data as proxies of Laurentide and Greenland/European ice sheets discharges, we suggest that for Termination II, MIS 8 and MIS 16, the Heinrich-like and Greenland/European ice sheets discharge events delay the response of monsoons and thus $\delta^{18}O_{atm}$ with respect to precessional forcing. By contrast, when we detect the smallest offsets between $\delta O_2/N_2$ and $\delta^{18}O_{atm}$ (Figure 4), no discharge events are observed within our marine core records. We therefore explain the minimum lag between $\delta^{18}O_{atm}$ and precession during MIS 6–7, the end of MIS 9, the end of MIS14-start of MIS 15 and the end of MIS 17 by the combination of three factors: minimum effects of ice volume changes (due to intermediate ice sheet extent), strong impact of precession on monsoons (due to high eccentricity), and the absence of ice sheets discharge event.

In summary, our datasets suggest that the offset between $\delta^{18}\mathrm{O}_{\mathrm{atm}}$ and precession can vary between 1 ka to more than 6 ka, with minimum values during periods of strong eccentricity and intermediate ice volume (no discharge events). This varying lag results from the complex interplay of orbital and millennial variations affecting changes in sea–water isotopic composition, tropical water cycle, and biosphere productivity. The delay identified over Termination I and II may not apply for earlier transitions without Heinrich-like events. Consequently, the phase lag of Termination I may provide an upper estimate for the associated uncertainty range.

4 Conclusions and perspectives

We have presented new measurements of $\delta\mathrm{O}_2/\mathrm{N}_2$ and $\delta^{18}\mathrm{O}_{\mathrm{atm}}$ performed on well–conserved ice from EDC over MIS 5 and between 340–800 ka. As a result, we now have a new reference $\delta\mathrm{O}_2/\mathrm{N}_2$ curve between 340–800 ka with a mean resolution of 2.08 ka, confirming earlier observations about a decreasing trend over the last 800 ka and timing of orbital scale variations. The spectral analysis of the new $\delta\mathrm{O}_2/\mathrm{N}_2$ curve between 340–800 ka showed for the first time a significant peak in the periodicity band characterizing eccentricity and glacial–interglacial variations, hence suggesting that processes other than local summer insolation do impact $\delta\mathrm{O}_2/\mathrm{N}_2$ on glacial–interglacial scales. This should motivates further studies to unveil the processes at play both for long term trends and at glacial–interglacial / eccentricity timescales.

Thanks to our comprehensive datasets, we have been able for the first time to compare the sequence of events between water stable isotopes, $\delta\mathrm{O}_2/\mathrm{N}_2$ and $\delta^{18}\mathrm{O}_{\mathrm{atm}}$ for three Antarctic ice cores (EDC, Vostok and Dome F), over MIS 5. Significant differences have been observed, which cannot be entirely explained by differences in resolution or by the corrections applied on $\delta\mathrm{O}_2/\mathrm{N}_2$ records of Dome F and Vostok. The combination of $\delta\mathrm{O}_2/\mathrm{N}_2$ records from the three sites has permitted to estimate the uncertainty of $\delta\mathrm{O}_2/\mathrm{N}_2$ orbital tuning method to be in the order of 3-4 ka. Moreover, we have evidenced that the relative timing between $\delta\mathrm{O}_2/\mathrm{N}_2$ and water isotopic composition may vary from site to site. This may be due to an influence of local climatic parameters on the $\delta\mathrm{O}_2/\mathrm{N}_2$. This demonstrates the interest of the multi-proxy, multi-ice cores chronology approach, which is therefore crucial to correctly assess the uncertainties associated with individual age markers. The mechanisms responsible for local $\delta\mathrm{O}_2/\mathrm{N}_2$ variations still remain to be understood. This is particularly important over periods of low eccentricity when the insolation variations are not well imprinted in the $\delta\mathrm{O}_2/\mathrm{N}_2$ records (350–450 ka and 700–800 ka). The $\delta\mathrm{O}_2/\mathrm{N}_2$ orbital tuning method should not be used alone during these periods.

We have calculated the offset between $\delta\mathrm{O}_2/\mathrm{N}_2$ and $\delta^{18}\mathrm{O}_{\mathrm{atm}}$ over the last 800 ka by coupling Vostok and EDC data. This lag has varied from 1 to more than 6 ka with minimum values occurring during MIS 6–7, the end of MIS 9, the end of MIS 14-start of MIS 15 and the end of MIS 17, corresponding to periods of high eccentricity and intermediate ice–sheet extent. Based on results observed over MIS 5, we make the assumption that $\delta O_2/N_2$ is more or less synchronous with summer solstice insolation and that the $\delta O_2/N_2$–$\delta^{18}O_{atm}$ varying lag is mainly induced by variations in the relationship between $\delta^{18}O_{atm}$ and precession. It has been shown over Terminations I and II that the $\delta^{18}O_{atm}$ response to precession can be delayed during Heinrich events, associated with weak monsoon intervals. The small values of the phase delay observed during MIS 6–7, the end of MIS 9, the end of MIS 14-start of MIS 15 and the end of MIS 17 are therefore attributed to a lack of ice sheets discharge events during these periods, combined with high eccentricity and intermediate ice sheet extent.

In order to refine this analysis, new measurements on well–conserved ice of $\delta O_2/N_2$ and $\delta^{18}O_{atm}$ are needed between 160–340 ka for the EDC ice core, and over the last 400 ka for Vostok and Dome F ice cores. Integrating Dome F on the AICC2012 age scale will be crucial to improve the Antarctic chronology. This methodology will then permit to investigate properly the causes of inter–site differences during MIS 5, and assess if similar features arise during other time periods. New measurements on well–conserved ice together with constraints on past changes in dust concentration and accumulation rates should allow us to assess whether there is any robust link between variables that can potentially affect metamorphism such as dust content and accumulation rate. Moreover, further studies are needed on processes affecting surface snow in order to better understand its metamorphism. Finally, it is crucial to better understand how the low latitude water cycle and biosphere productivity influence the $\delta^{18}O_{atm}$ and its lagged response to precession in order to estimate correctly the uncertainty associated with the $\delta^{18}O_{atm}$ orbital tuning methods. To do so, it is necessary to improve uncertainties associated with ice and marine cores. The development of multi-archives dating tool should permit to synchronize records from different archives and thus discuss in more details how the ice sheets discharge events influence the $\delta^{18}O_{atm}$ lag with precession. This will especially permit to directly link $\delta^{18}O_{atm}$ variations with absolutely dates speleothem records.

Appendix A: EDC $\delta O_2/N_2$ records

We have compared the $\delta O_2/N_2$ composite curve of Landais et al. (2012), corrected for gas loss, with our new record only measured on well–conserved ice (Figure A1). We observe nearly the same timing of variations. We conclude that the increased resolution and accuracy of our new dataset do not affect the position of mid–slope variations and therefore orbital tuning. The uncertainty associated with the mid–slope identification is always smaller than the uncertainty associated with $\delta O_2/N_2$ orbital tuning. Note that we have identified an error in the earlier composite curve due to the use of gas age instead of ice age for the time period 400 to 450 ka. This error has been corrected and explains the difference between our new record and the one of Landais et al. (2012). Compared to the Landais et al. (2012) composite curve, the new record presents smaller amplitudes of variations, possibly because of gas loss corrections. Our new data record a long term decrease of $\delta O_2/N_2$ over time of 0.78 ± 0.08 ‰/100 ka, which is very close to the long term decrease of 0.86 ± 0.14 ‰/100 ka, deduced from the Landais et al. (2012) composite curve.

Appendix B: Estimation of the uncertainty associated with orbital tuning

In this paper we propose an uncertainty estimation for the $\delta O_2/N_2$ orbital tuning method based on the comparison of $\delta O_2/N_2$ records of EDC, Vostok and Dome F over MIS 5. In order to estimate the uncertainty in the identification of minima, maxima or mid-slopes in the $\delta O_2/N_2$ records we have treated the three $\delta O_2/N_2$ records as follow:

1. the raw data,
2. a 3–points running average of the $\delta O_2/N_2$,
3. reinterpolation of the data with a time step corresponding to the mean resolution of each $\delta O_2/N_2$ record (2.37 ka for EDC, 1.87 ka for Vostok and 1.69 ka for Dome F),
4. filtering of the reinterpolated data (piecewise linear shape with a slope bandwidth of 10^{-9} a^{-1} and between 15-100 ka using Analyseries, (Paillard et al., 1996)).

We have identified the minima, mid-slopes and maxima for the 4 $\delta O_2/N_2$ treated records of the different sites. We were then able to calculate the mean age and standard deviation for each of these identification (Table 2). The final uncertainty associated with the identification of the extrema and mid-slopes of the $\delta O_2/N_2$ records has been obtained after considering also the resolution of the records and the uncertainty of their respective chronologies (AICC2012 for EDC and Vostok, DFO-2006 for Dome F, Table 2). The results are illustrated on Figure B1 where the pink lines and shaded zones correspond to the mean age and uncertainty of minima and maxima of $\delta O_2/N_2$ for EDC (top), Vostok (middle) and Dome F (bottom). The grey bars indicate the position of minima and maxima as identified in the local summer solstice insolation for comparison.

Appendix C: Volcanic matching between EDC and Dome F

We have performed a new synchronisation based on the volcanic synchronisation of EDC and Dome F of Fujita et al. (2015). We were then able to transfer (1) Dome F data ($\delta^{18}O_{ice}$, $\delta O_2/N_2$ and $\delta^{18}O_{atm}$) from DFO-2006 to AICC2012 and (2) EDC data from AICC2012 to DFO-2006 chronology (Figure C1). As can be seen on Figure C1, there are numerous volcanic markers (red markers on top) between these two cores over the whole MIS5 period. This volcanic synchronization is robust and independent of any climatic assumption. As noted by Fujita et al. (2015), this volcanic synchronization does not resolve the difference of ice isotopic composition over the glacial inception at these two sites. Potential causes for this large age difference between the DFO-2006 and AICC2012 chronologies are: an overestimation of the surface mass balance in the glaciological approach and/or an error in one of Dome F $\delta O_2/N_2$ age constraint by 3 ka.

Acknowledgements. We thank Jean–Robert Petit and Laurent Arnaud for the help with the surface temperature data of Vostok and EDC. We thank James Channell for the marine cores data. The present research project No 902 has been performed at Concordia Station and was supported by the French Polar Institute (IPEV). This project was funded by the “Fondation de France Ars Cuttoli" and the “ANR Citronnier". The research leading to these results has received funding from the European Union’s Seventh Framework programme (FP7/2007-2013) under grant agreement no 243908, “Past4Future. Climate change – Learning from the past climate". This is Past4Future contribution number XX. This is LSCE contribution no XX.

References

Battle, M., Bender, M., Sowers, T., Tans, P. P., Butler, J. H., Elkins, J. W., Ellis, J. T., Conway, T., Zhang, N., Lang, P., and Clarket, A. D.: Atmospheric gas concentrations over the past century measured in air from firn at the South Pole, Nature, 383, 231–235, doi:10.1038/383231a0, 1996.

Bazin, L., Landais, A., Lemieux-Dudon, B., Toyé Mahamadou Kele, H., Veres, D., Parrenin, F., Martinerie, P., Ritz, C., Capron, E., Lipenkov, V., Loutre, M.-F., Raynaud, D., Vinther, B., Svensson, A., Rasmussen, S., Severi, M., Blunier, T., Leuenberger, M., Fischer, H., Masson-Delmotte, V., Chappellaz, J., and Wolff, E.: An optimized multi-proxies, multi-site Antarctic ice and gas orbital chronology (AICC2012): 120-800 ka, Climate of the Past, 9, 1715–1731, doi:10.5194/cp-9-1715-2013, 2013.

Bender, M., Sowers, T., and Labeyrie, L.: The Dole effect and its variations during the last 130,000 years as measured in the Vostok ice core, Global Biogeochemical Cycles, 8, 363–376, doi:10.1029/94GB00724, 1994.

Bender, M., Sowers, T., and Lipenkov, V.: On the concentrations of O_2, N_2, and Ar in trapped gases from ice cores, Journal of Geophysical Research: Atmospheres, 100, 18 651–18 660, doi:10.1029/94JD02212, 1995.

Bender, M. L.: Orbital tuning chronology for the Vostok climate record supported by trapped gas composition, Earth and Planetary Science Letters, 204, 275–289, doi:10.1016/S0012-821X(02)00980-9, 2002.

Braconnot, P., Marzin, C., Grégoire, L., Mosquet, E., and Marti, O.: Monsoon response to changes in Earth's orbital parameters: comparisons between simulations of the Eemian and of the Holocene, Climate of the Past, 4, 281–294, doi:doi:10.5194/cp-4-281-2008, 2008.

Buiron, D., Chappellaz, J., Stenni, B., Frezzotti, M., Baumgartner, M., Capron, E., Landais, A., Lemieux-Dudon, B., Masson-Delmotte, V., Montagnat, M., Parrenin, F., and Schilt, A.: TALDICE-1 age scale of the Talos Dome deep ice core, East Antarctica, Climate of the Past, 7, 1–16, doi:10.5194/cp-7-1-2011, 2011.

Caley, T., Malaizé, B., Revel, M., Ducassou, E., Wainer, K., Ibrahim, M., Shoeaib, D., Migeon, S., and Marieu, V.: Orbital timing of the Indian, East Asian and African boreal monsoons and the concept of a 'global monsoon', Quaternary Science Reviews, 30, 3705–3715, doi:10.1016/j.quascirev.2011.09.015, 2011.

Channell, J., Hodell, D., Romero, O., Hillaire-Marcel, C., de Vernal, A., Stoner, J., Mazaud, A., and Röhl, U.: A 750-kyr detrital-layer stratigraphy for the North Atlantic (IODP Sites U1302–U1303, Orphan Knoll, Labrador Sea) , Earth and Planetary Science Letters, 317–318, 218 – 230, doi:10.1016/j.epsl.2011.11.029, 2012.

Channell, J. E. T. and Hodell, D. A.: Magnetic signatures of Heinrich-like detrital layers in the Quaternary of the North Atlantic, Earth and Planetary Science Letters, 369, 260–270, doi:10.1016/j.epsl.2013.03.034, 2013.

Cheng, H., Edwards, R. L., Broecker, W. S., Denton, G. H., Kong, X., Wang, Y., Zhang, R., and Wang, X.: Ice Age Terminations, Science, 326, 248–252, doi:10.1126/science.1177840, 2009.

Denton, G. H., Anderson, R. F., Toggweiler, J. R., Edwards, R. L., Schaefer, J. M., and Putnam, A. E.: The Last Glacial Termination, Science, 328, 1652–1656, doi:10.1126/science.1184119, 2010.

Dreyfus, G. B., Parrenin, F., Lemieux-Dudon, B., Durand, G., Masson-Delmotte, V., Jouzel, J., Barnola, J.-M., Panno, L., Spahni, R., Tisserand, A., Siegenthaler, U., and Leuenberger, M.: Anomalous flow below 2700 m in the EPICA Dome C ice core detected using δ^{18}O of atmospheric oxygen measurements, Climate of the Past, 3, 341–353, doi:10.5194/cp-3-341-2007, 2007.

Dreyfus, G. B., Raisbeck, G. M., Parrenin, F., Jouzel, J., Guyodo, Y., Nomade, S., and Mazaud, A.: An ice core perspective on the age of the Matuyama-Brunhes boundary, Earth and Planetary Science Letters, 274, 151–156, doi:10.1016/j.epsl.2008.07.008, 2008.

Freitag, J., Kipfstuhl, S., Laepple, T., and Wilhelms, F.: Impurity-controlled densification: a new model for stratified polar firn, Journal of Glaciology, 59, 1163–1169, doi:doi:10.3189/2013JoG13J042, 2013.

Fujita, S., Okuyama, J., Hori, A., and Hondoh, T.: A mechanism for local insolation modulation of gas transport conditions during bubble close off, J. Geophys. Res., 114, F03 023, 2009.

Fujita, S., Enomoto, H., Fukui, K., Iizuka, Y., Motoyama, H., Nakazawa, F., Sugiyama, S., and Surdyk, S.: Formation and metamorphism of stratified firn at sites located under spatial variations of accumulation rate and wind speed on the East Antarctic ice divide near Dome Fuji, The Cryosphere Discussions, 6, 1205–1267, doi:10.5194/tcd-6-1205-2012, 2012.

Fujita, S., Parrenin, F., Severi, M., Motoyama, H., and Wolff, E.: Volcanic synchronization of Dome Fuji and Dome C Antarctic deep ice cores over the past 216 kyr, Climate of the Past, 11, 1395–1416, 2015.

Hodell, D. A., Channell, J. E. T., Curtis, J. H., Romero, O. E., and RöHl, U.: Onset of "Hudson Strait" Heinrich events in the eastern North Atlantic at the end of the middle Pleistocene transition ($\sim$640 ka)?, Paleoceanography, 23, 4218, doi:10.1029/2008PA001591, 2008.

Hörhold, M., Laepple, T., Freitag, J., Bigler, M., Fischer, H., and Kipfstuhl, S.: On the impact of impurities on the densification of polar firn , Earth and Planetary Science Letters, 325–326, 93 – 99, doi:10.1016/j.epsl.2011.12.022, 2012.

Huber, C., Beyerle, U., Leuenberger, M., Schwander, J., Kipfer, R., Spahni, R., Severinghaus, J. P., and Weiler, K.: Evidence for molecular size dependent gas fractionation in firn air derived from noble gases, oxygen, and nitrogen measurements, Earth and Planetary Science Letters, 243, 61–73, doi:10.1016/j.epsl.2005.12.036, 2006.

Hutterli, M. A., Schneebeli, M., Freitag, J., Kipfstuhl, J., and Roth-lisberger, R.: Impact of local insolation on snow metamorphism and ice core records, Physics of ice core records II, T. Hondoh, Hokkaido University Press, 223–232, 2010.

Imbrie, J. and Imbrie, J. Z.: Modeling the Climatic Response to Orbital Variations, Science, 207, 943–953, doi:10.1126/science.207.4434.943, 1980.

Jouzel, J., Waelbroeck, C., Malaize, B., Bender, M., Petit, J., Stievenard, M., Barkov, N., Barnola, J., King, T., Kotlyakov, V., Lipenkov, V., Lorius, C., Raynaud, D., Ritz, C., and Sowers, T.: Climatic interpretation of the recently extended Vostok ice records, Climate Dynamics, 12, 513–521, doi:10.1007/BF00207935, 1996.

Jouzel, J., Hoffmann, G., Parrenin, F., and Waelbroeck, C.: Atmospheric oxygen 18 and sea-level changes, Quaternary Science Reviews, 21, 307–314, doi:10.1016/S0277-3791(01)00106-8, 2002.

Jouzel, J., Masson-Delmotte, V., Cattani, O., Dreyfus, G., Falourd, S., Hoffmann, G., Minster, B., Nouet, J., Barnola, J. M., Chappellaz, J., Fischer, H., Gallet, J. C., Johnsen, S., Leuenberger, M., Loulergue, L., Luethi, D., Oerter, H., Parrenin, F., Raisbeck, G., Raynaud, D., Schilt, A., Schwander, J., Selmo, E., Souchez, R., Spahni, R., Stauffer, B., Steffensen, J. P., Stenni, B., Stocker, T. F., Tison, J. L., Werner, M., and Wolff, E. W.: Orbital and Millennial Antarctic Climate Variability over the Past 800,000 Years, Science, 317, 793–, doi:10.1126/science.1141038, 2007.

Kawamura, K., Parrenin, F., Lisiecki, L., Uemura, R., Vimeux, F., Severinghaus, J. P., Hutterli, M. A., Nakazawa, T., Aoki, S., Jouzel, J., Raymo, M. E., Matsumoto, K., Nakata, H., Motoyama, H., Fujita, S., Goto-Azuma, K., Fujii, Y., and Watanabe, O.: Northern Hemisphere forcing of climatic cycles in Antarctica over the past 360,000years, Nature, 448, 912–916, doi:10.1038/nature06015, 2007.

Kobashi, T., Ikeda-Fukazawa, T., Suwa, M., Schwander, J., Kameda, T., Lundin, J., Hori, A., Döring, M., and Leuenberger, M.: Post bubble-closeoff fractionation of gases in polar firn and ice cores: effects of accumulation rate on permeation through overloading presure, Atmospheric Chemistry and Physics Discussions, 15, 15 711–15 753, 2015.

Lambert, F., Delmonte, B., Petit, J. R., Bigler, M., Kaufmann, P. R., Hutterli, M. A., Stocker, T. F., Ruth, U., Steffensen, J. P., and Maggi, V.: Dust-climate couplings over the past 800,000 years from the EPICA Dome C ice core, Nature, 452, 616–619, doi:10.1038/nature06763, 2008.

Landais, A., Caillon, N., Severinghaus, J., Jouzel, J., and Masson- Delmotte, V.: Analyses isotopiques à haute précision de l'air piégé dans les glaces polaires pour la quantification des variations rapides de température: méthodes et limites, Notes des activités instrumentales de l'IPSL, 39, 2003.

Landais, A., Masson-Delmotte, V., Combourieu Nebout, N., Jouzel, J., Blunier, T., Leuenberger, M., Dahl-Jensen, D., and Johnsen, S.: Millenial scale variations of the isotopic composition of atmospheric oxygen over Marine Isotopic Stage 4, Earth and Planetary Science Letters, 258, 101–113, doi:10.1016/j.epsl.2007.03.027, 2007.

Landais, A., Dreyfus, G., Capron, E., Masson-Delmotte, V., Sanchez-Goñi, M., Desprat, S., Hoffmann, G., Jouzel, J., Leuenberger, M., and Johnsen, S.: What drives the millennial and orbital variations of $\delta^{18}O_{atm}$?, Quaternary Science Reviews, 29, 235–246, doi:10.1016/j.quascirev.2009.07.005, 2010.

Landais, A., Dreyfus, G., Capron, E., Pol, K., Loutre, M. F., Raynaud, D., Lipenkov, V. Y., Arnaud, L., Masson-Delmotte, V., Paillard, D., Jouzel, J., and Leuenberger, M.: Towards orbital dating of the EPICA Dome C ice core using $\delta O_2/N_2$, Climate of the Past, 8, 191–203, doi:10.5194/cp-8-191-2012, 2012.

Landais, A., Dreyfus, G., Capron, E., Jouzel, J., Masson-Delmotte, V., Roche, D., prie, F., caillon, N., Chappellaz, J., Leuenberger, M., and lourantou, A. and Parrenin, F. and Raynaud, D. and Teste, G.: Two-phase change in CO_2, Antarctic temperature and global climate during Termination II, Nature Geoscience, 6, 1062–1065, doi:10.1038/ngeo1985, 2013.

Laskar, J., Robutel, P., Joutel, F., Gastineau, M., Correia, A. C. M., and Levrard, B.: A long-term numerical solution for the insolation quantities of the Earth, Astronomy & Astrophysics, 428, 261–285, doi:10.1051/0004-6361:20041335, 2004.

Lefebvre, E., Arnaud, L., Ekaykin, A., Lipenkov, V., Picard, G., and Petit, J.-R.: Snow temperature measurements at Vostok station from an autonomous recording system (TAUTO): preliminary results from the first year operation, 4, 138–145, 2012.

Lemieux-Dudon, B., Blayo, E., Petit, J.-R., Waelbroeck, C., Svensson, A., Ritz, C., Barnola, J.-M., Narcisi, B. M., and Parrenin, F.: Consistent dating for Antarctic and Greenland ice cores, Quaternary Science Reviews, 29, 8–20, doi:10.1016/j.quascirev.2009.11.010, 2010.

Leuenberger, M. C.: Modeling the signal transfer of seawater δ^{18}O to the δ^{18}O of atmospheric oxygen using a diagnostic box model for the terrestrial and marine biosphere, J. Geophys. Res., 102, 26 841–26 850, doi:10.1029/97JC00160, 1997.

Libois, Q., Picard, G., Arnaud, L., Morin, S., and Brun, E.: Modeling the impact of snow drift on the decameter-scale variability of snow properties on the Antarctic Plateau, Journal of Geophysical Research: Atmospheres, 119, 11,662–11,681, 2014.

Lipenkov, V. Y., Raynaud, D., Loutre, M. F., and Duval, P.: On the potential of coupling air content and O_2/N_2 from trapped air for establishing an ice core chronology tuned on local insolation, Quaternary Science Reviews, 30, 3280–3289, doi:10.1016/j.quascirev.2011.07.013, 2011.

Lisiecki, L. E. and Raymo, M.: A Pliocene-Pleistocene stack of 57 globally distributed benthic $\delta^{18}O$ records, Paleoceanography, 20, 1003, 2005.

Loulergue, L., Schilt, A., Spahni, R., Masson-Delmotte, V., Blunier, T., Lemieux, B., Barnola, J.-M., Raynaud, D., Stocker, T. F., and Chappellaz, J.: Orbital and millennial-scale features of atmospheric CH_4 over the past 800,000years, Nature, 453, 383–386, doi:10.1038/nature06950, 2008.

Lüthi, D., Le Floch, M., Bereiter, B., Blunier, T., Barnola, J.-M., Siegenthaler, U., Raynaud, D., Jouzel, J., Fischer, H., Kawamura, K., and Stocker, T. F.: High-resolution carbon dioxide concentration record 650,000-800,000 years before present, Nature, 453, 379–382, doi:10.1038/nature06949, 2008.

Malaizé, B., Paillard, D., Jouzel, J., and Raynaud, D.: The Dole effect over the last two glacial-interglacial cycles, J. Geophys. Res., 104, 14 199–14 208, doi:10.1029/1999JD900116, 1999.

Marzin, C., Kallel, N., Kageyama, M., Duplessy, J.-C., and Braconnot, P.: Glacial fluctuations of the Indian monsoon and their relationship with North Atlantic abrupt climate change: new data and climate experiments, Climate of the Past, 9, 2135–2151, doi:10.5194/cp-9-2135-2013, 2013.

Masson-Delmotte, V., Stenni, B., Pol, K., Braconnot, P., Cattani, O., Falourd, S., Kageyama, M., Jouzel, J., Landais, A., Minster, B., Barnola, J. M., Chappellaz, J., Krinner, G., Johnsen, S., Röthlisberger, R., Hansen, J., Mikolajewicz, U., and Otto-Bliesner, B.: EPICA Dome C record of glacial and interglacial intensities, Quaternary Science Reviews, 29, 113–128, doi:10.1016/j.quascirev.2009.09.030, 2010.

Masson-Delmotte, V., Buiron, D., Ekaykin, A., Frezzotti, M., Gallée, H., Jouzel, J., Krinner, G., Landais, A., Motoyama, H., Oerter, H., Pol, K., Pollard, D., Ritz, C., Schlosser, E., Sime, L. C., Sodemann, H., Stenni, B., Uemura, R., and Vimeux, F.: A comparison of the present and last interglacial periods in six Antarctic ice cores, Climate of the Past, 7, 397–423, doi:10.5194/cp-7-397-2011, 2011.

Meese, D. A., Gow, A. J., Grootes, P., Stuiver, M., Mayewski, P. A., Zielinski, G. A., Ram, M., Taylor, K. C., and Waddington, E. D.: The Accumulation Record from the GISP2 Core as an Indicator of Climate Change Throughout the Holocene, Science, 266, 1680–1682, doi:10.1126/science.266.5191.1680, 1994.

Paillard, D., Labeyrie, L., and Yiou, P.: Macintosh Program performs time-series analysis, EOS Transactions, 77, 379–379, doi:10.1029/96EO00259, 1996.

Parrenin, F., Jouzel, J., Waelbroeck, C., Ritz, C., and Barnola, J.-M.: Dating the Vostok ice core by an inverse method, J. Geophys. Res., 106, 31 837–31 852, doi:10.1029/2001JD900245, 2001.

Parrenin, F., Rémy, F., Ritz, C., Siegert, M. J., and Jouzel, J.: New modeling of the Vostok ice flow line and implication for the glaciological chronology of the Vostok ice core, Journal of Geophysical Research (Atmospheres), 109, D20102, doi:10.1029/2004JD004561, 2004.

Parrenin, F., Barnola, J.-M., Beer, J., Blunier, T., Castellano, E., Chappellaz, J., Dreyfus, G., Fischer, H., Fujita, S., Jouzel, J., Kawamura, K., Lemieux-Dudon, B., Loulergue, L., Masson-Delmotte, V., Narcisi, B., Petit, J.-R., Raisbeck, G., Raynaud, D., Ruth, U., Schwander, J., Severi, M., Spahni, R., Steffensen, J. P., Svensson, A., Udisti, R., Waelbroeck, C., and Wolff, E.: The EDC3 chronology for the EPICA Dome C ice core, Climate of the Past, 3, 485–497, doi:10.5194/cp-3-485-2007, 2007.

Parrenin, F., Bazin, L., Capron, E., Landais, A., Lemieux-Dudon, B., and Masson-Delmotte, V.: IceChrono1: a probabilistic model to compute a common and optimal chronology for several ice cores, Geoscientific Model Development, 8, 1473–1492, 2015.

Petit, J. R., Jouzel, J., Raynaud, D., Barkov, N. I., Barnola, J.-M., Basile, I., Bender, M., Chappellaz, J., Davis, M., Delaygue, G., Delmotte, M., Kotlyakov, V. M., Legrand, M., Lipenkov, V. Y., Lorius, C., Pépin, L., Ritz, C., Saltzman, E., and Stievenard, M.: Climate and atmospheric history of the past 420,000 years from the Vostok ice core, Antarctica, Nature, 399, 429–436, doi:10.1038/20859, 1999.

Picard, G., Domine, F., Krinner, G., Arnaud, L., and Lefebvre, E.: Inhibition of the positive snow-albedo feedback by precipitation in interior Antarctica, Nature Climate Change, 2, 795–798, doi:10.1038/nclimate1590, 2012.

Raynaud, D., Lipenkov, V., Lemieux-Dudon, B., Duval, P., Loutre, M.-F., and Lhomme, N.: The local insolation signature of air content in Antarctic ice. A new step toward an absolute dating of ice records, Earth and Planetary Science Letters, 261, 337–349, doi:10.1016/j.epsl.2007.06.025, 2007.

Reutenauer, C., Landais, A., Blunier, T., Bréant, C., Kageyama, M., Woillez, M.-C., Risi, C., Mariotti, V., and Braconnot, P.: Quantifying molecular oxygen isotope variations during a Heinrich stadial, Climate of the Past, 11, 1527–1551, 2015.

Schaaf, C. B., Wang, Z., and Strahler, A. H.: Commentary on Wang and Zender—MODIS snow albedo bias at high solar zenith angles relative to theory and to in situ observations in Greenland, Remote Sensing of Environment, 115, 1296 – 1300, doi:10.1016/j.rse.2011.01.002, 2011.

Severinghaus, J. P. and Battle, M. O.: Fractionation of gases in polar ice during bubble close-off: New constraints from firn air Ne, Kr and Xe observations, Earth and Planetary Science Letters, 244, 474–500, doi:10.1016/j.epsl.2006.01.032, 2006.

Severinghaus, J. P., Grachev, A., and Battle, M.: Thermal fractionation of air in polar firn by seasonal temperature gradients, Geochem. Geophys. Geosyst., 2, doi:10.1029/2000GC000146, 2001.

Severinghaus, J. P., Beaudette, R., Headly, M. A., Taylor, K., and Brook, E. J.: Oxygen-18 of O_2 Records the Impact of Abrupt Climate Change on the Terrestrial Biosphere, Science, 324, 1431–, doi:10.1126/science.1169473, 2009.

Shackleton, N. J., Hall, M. A., and Vincent, E.: Phase relationships between millennial-scale events 64,000-24,000 years ago, Paleoceanography, 15, 565–569, doi:10.1029/2000PA000513, 2000.

Sime, L. C., Wolff, E. W., Oliver, K. I. C., and Tindall, J. C.: Evidence for warmer interglacials in East Antarctic ice cores, Nature, 462, 342–345, doi:10.1038/nature08564, 2009.

Sowers, T., Bender, M., and Raynaud, D.: Elemental and isotopic composition of occluded O2 and N2 in polar ice, J. Geophys. Res., 94, 5137–5150, doi:10.1029/JD094iD04p05137, 1989.

Spahni, R., Chappellaz, J., Stocker, T. F., Loulergue, L., Hausammann, G., Kawamura, K., Flückiger, J., Schwander, J., Raynaud, D., Masson-Delmotte, V., and Jouzel, J.: Atmospheric Methane and Nitrous Oxide of the Late Pleistocene from Antarctic Ice Cores, Science, 310, 1317–1321, doi:10.1126/science.1120132, 2005.

Stenni, B., Masson-Delmotte, V., Selmo, E., Oerter, H., Meyer, H., Röthlisberger, R., Jouzel, J., Cattani, O., Falourd, S., Fischer, H., Hoffmann, G., Iacumin, P., Johnsen, S. J., Minster, B., and Udisti, R.: The deuterium excess records of EPICA Dome C and Dronning Maud Land ice cores (East Antarctica), Quaternary Science Reviews, 29, 146–159, doi:10.1016/j.quascirev.2009.10.009, 2010.

Suwa, M. and Bender, M. L.: O_2/N_2 ratios of occluded air in the GISP2 ice core, Journal of Geophysical Research (Atmospheres), 113, D11119, doi:10.1029/2007JD009589, 2008a.

Suwa, M. and Bender, M. L.: Chronology of the Vostok ice core constrained by O_2/N_2 ratios of occluded air, and its implication for the Vostok climate records, Quaternary Science Reviews, 27, 1093–1106, doi:10.1016/j.quascirev.2008.02.017, 2008b.

Svensson, A., Andersen, K. K., Bigler, M., Clausen, H. B., Dahl-Jensen, D., Davies, S. M., Johnsen, S. J., Muscheler, R., Parrenin, F., Rasmussen, S. O., Röthlisberger, R., Seierstad, I., Steffensen, J. P., and Vinther, B. M.: A 60 000 year Greenland stratigraphic ice core chronology, Climate of the Past, 4, 47–57, 2008.

Town, M. S., Waddington, E. D., Walden, V. P., and Warren, S. G.: Temperatures, heating rates and vapour pressures in near-surface snow at the South Pole, Journal of Glaciology, 54, 487–498, doi:10.3189/002214308785837075, 2008.

Uemura, R., Masson-Delmotte, V., Jouzel, J., Landais, A., Motoyama, H., and Stenni, B.: Ranges of moisture-source temperature estimated from Antarctic ice cores stable isotope records over glacial-interglacial cycles, Climate of the Past, 8, 1109–1125, doi:10.5194/cp-8-1109-2012, 2012.

Veres, D., Bazin, L., Landais, A., Toye Mahamadou Kele, H., Lemieux-Dudon, B., Parrenin, F., Martinerie, P., Blayo, E., Blunier, T., Capron, E., Chappellaz, J., Rasmussen, S., Severi, M., Svensson, A., Vinther, B., and Wolff, E.: The Antarctic ice core chronology (AICC2012): an optimized multi-parameter and multi-site dating approach for the last 120 thousand years, Climate of the Past, 9, 1733–1748, doi:10.5194/cp-9-1733-2013, 2013.

Waelbroeck, C., Frank, N., Jouzel, J., Parrenin, F., Masson-Delmotte, V., and Genty, D.: Transferring radiometric dating of the last interglacial sea level high stand to marine and ice core records, Earth and Planetary Science Letters, 265, 183–194, doi:10.1016/j.epsl.2007.10.006, 2008.

Wang, Y., Cheng, H., Edwards, R. L., Kong, X., Shao, X., Chen, S., Wu, J., Jiang, X., Wang, X., and An, Z.: Millennial- and orbital-scale changes in the East Asian monsoon over the past 224,000years, Nature, 451, 1090–1093, doi:10.1038/nature06692, 2008.

Wang, Y. J., Cheng, H., Edwards, R. L., An, Z. S., Wu, J. Y., Shen, C.-C., and Dorale, J. A.: A High-Resolution Absolute-Dated Late Pleistocene Monsoon Record from Hulu Cave, China, Science, 294, 2345–2348, doi:10.1126/science.1064618, 2001.

Witrant, E., Martinerie, P., Hogan, C., Laube, J. C., Kawamura, K., Capron, E., Montzka, S. A., Dlugokencky, E. J., Etheridge, D., Blunier, T., and Sturges, W. T.: A new multi-gas constrained model of trace gas non-homogeneous transport in firn: evaluation and behaviour at eleven polar sites, Atmospheric Chemistry and Physics, 12, 11 465–11 483, 2012.

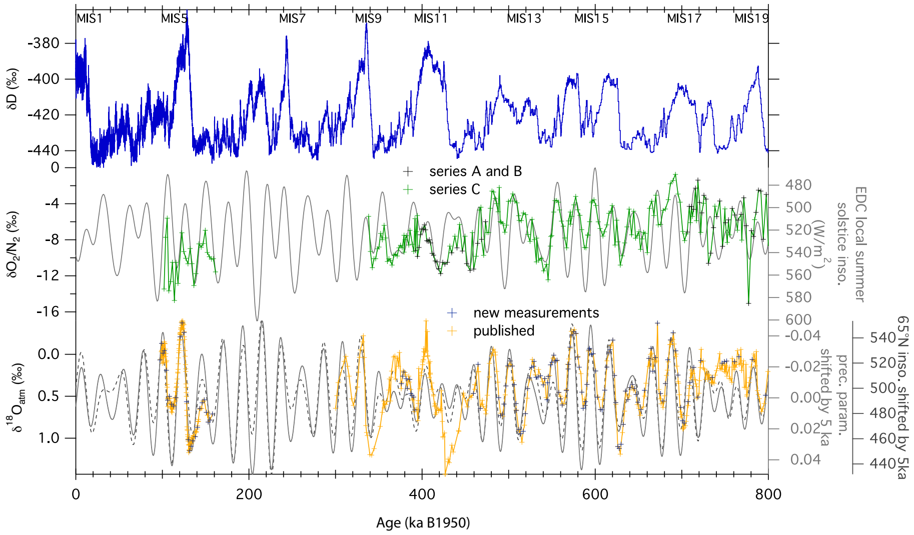

Figure 1. Top: EDC ice core record of water stable isotopes (δD, Jouzel et al., 2007). Middle: EDC record of $\delta O_2/N_2$ (black: Landais et al. (2012), green: this study) and local summer solstice insolation (grey, reversed axis). Bottom: EDC record of $\delta^{18}O_{atm}$(reversed vertical scale) (orange: Dreyfus et al. (2007, 2008); Landais et al. (2013), blue: this study), precession parameter (grey, reversed axis) and 65°N summer solstice insolation (dashed grey) both shifted by 5 ka. All EDC records are presented on the AICC2012 chronology (Bazin et al., 2013; Veres et al., 2013). The orbital parameters are calculated using the Laskar et al. (2004) solution, with the Analyseries software (Paillard et al., 1996).

Table 1. Summary of present day local conditions at Vostok, Dome F and EDC (Masson-Delmotte et al., 2011; Kawamura et al., 2007; Landais et al., 2012; Lefebvre et al., 2012, this study)

Site	Lat. Long.	Elevation (m a.s.l.)	Nb of days after 21 Dec. for max temp.	Mean albedo	Accu. rate (cm weq/yr)	Mean annual temp. (°C)	10 m wind speed (m/s)
Vostok	78°28'S 106°48'E	3488	10	0.83	2.15	−55.3	4.2
Dome F	77°19'S 39°40'E	3810	0	0.80	2.3	−57.0	2.9
EDC	75°06'S 123°21'E	3233	5 – 20	0.83	∼2.5	−54.5	5.4

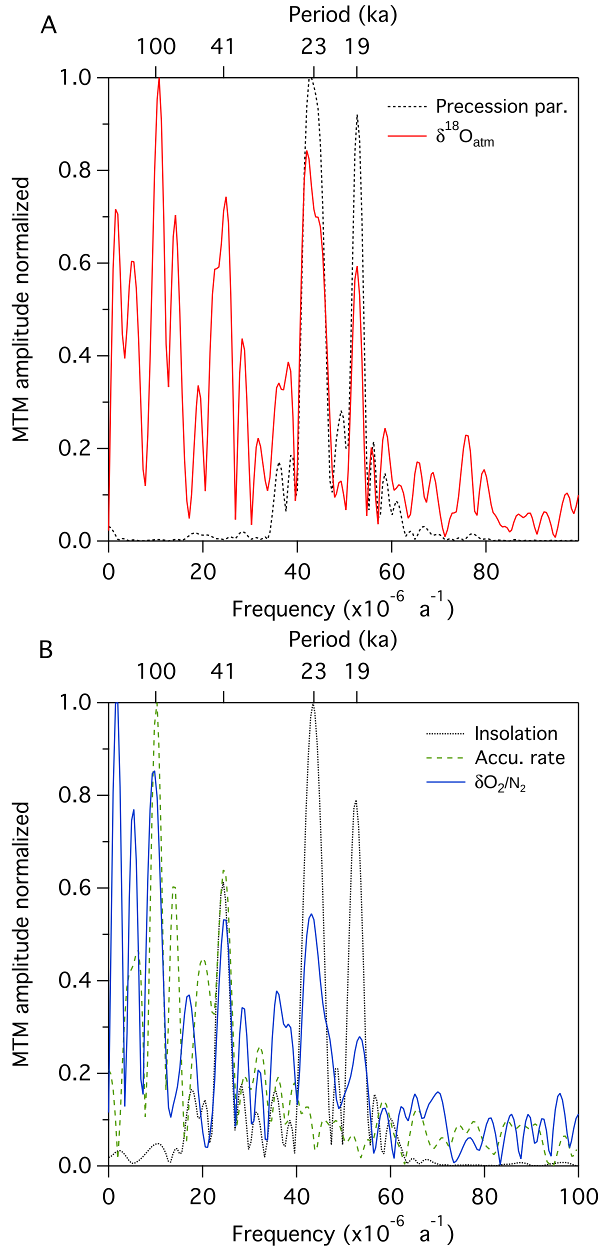

Figure 2. Spectral analysis using the Multi–Taper Method with an interpolation step of 1 ka, obtained with Analyseries (Paillard et al., 1996). Amplitudes are normalized by the maximum value of each serie. (a) $\delta^{18}\mathrm{O}_{\mathrm{atm}}$ between 300–800 ka (red) presented with the precession parameter (grey). (b) $\delta\mathrm{O}_2/\mathrm{N}_2$ between 340–800 ka (blue) presented with local summer solstice insolation (grey) and AICC2012 accumulation rate (dashed green). Periods corresponding to significant peaks (F-test$>90\%$) are indicated on the upper horizontal axis.

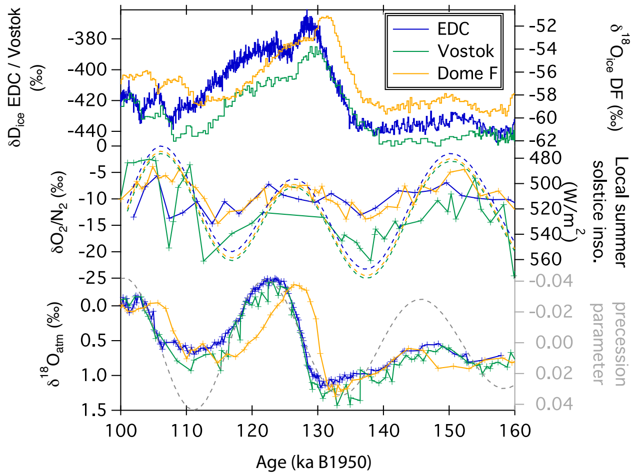

Figure 3. Inter–comparison of Vostok (green), Dome F (yellow) and EDC (blue) data covering MIS 5. Vostok and EDC data are presented on AICC2012 (Bazin et al., 2013; Veres et al., 2013) and Dome F on the DFO-2006 chronology (Kawamura et al., 2007). Top: water isotopic composition (Vostok $\delta^{18}\mathrm{O}_{\mathrm{ice}}$: Petit et al. (1999), Dome F $\delta^{18}\mathrm{O}_{\mathrm{ice}}$: Kawamura et al. (2007), EDC δD: Jouzel et al. (2007)). Middle: $\delta\mathrm{O}_2/\mathrm{N}_2$ records and local summer solstice insolation at each site (Suwa and Bender, 2008b; Kawamura et al., 2007, this study). Bottom: $\delta^{18}\mathrm{O}_{\mathrm{atm}}$ and precession parameter shifted by 5 ka (Suwa and Bender, 2008b; Kawamura et al., 2007; Landais et al., 2013, this study).

Table 2. Mean age and uncertainty calculated for minima, mid-slopes ans maxima in the $\delta\mathrm{O}_2/\mathrm{N}_2$ records of EDC, Vostok and Dome F over MIS 5.

		max 1	mid	min 1	mid	max 2	mid	min 2	mid	max 3
EDC	mean (ka)	104.7	107.7	114	119	123.8	131.8	136	141.3	148.3
	error (ka)	3.0	3.0	3.0	2.9	3.0	3.2	3.4	3.7	4.1
Vostok	mean (ka)	104.8	110.8	115	119	126.3	133.3	137	144.5	152.5
	error (ka)	2.7	2.5	2.7	2.7	2.8	2.8	3.2	3.4	3.6
Dome F	mean (ka)	106.5	112	115.8	120.3	126.5	132	138	144.5	151
	error (ka)	2.8	2.7	2.7	2.7	3.0	2.9	2.9	4.4	4.4

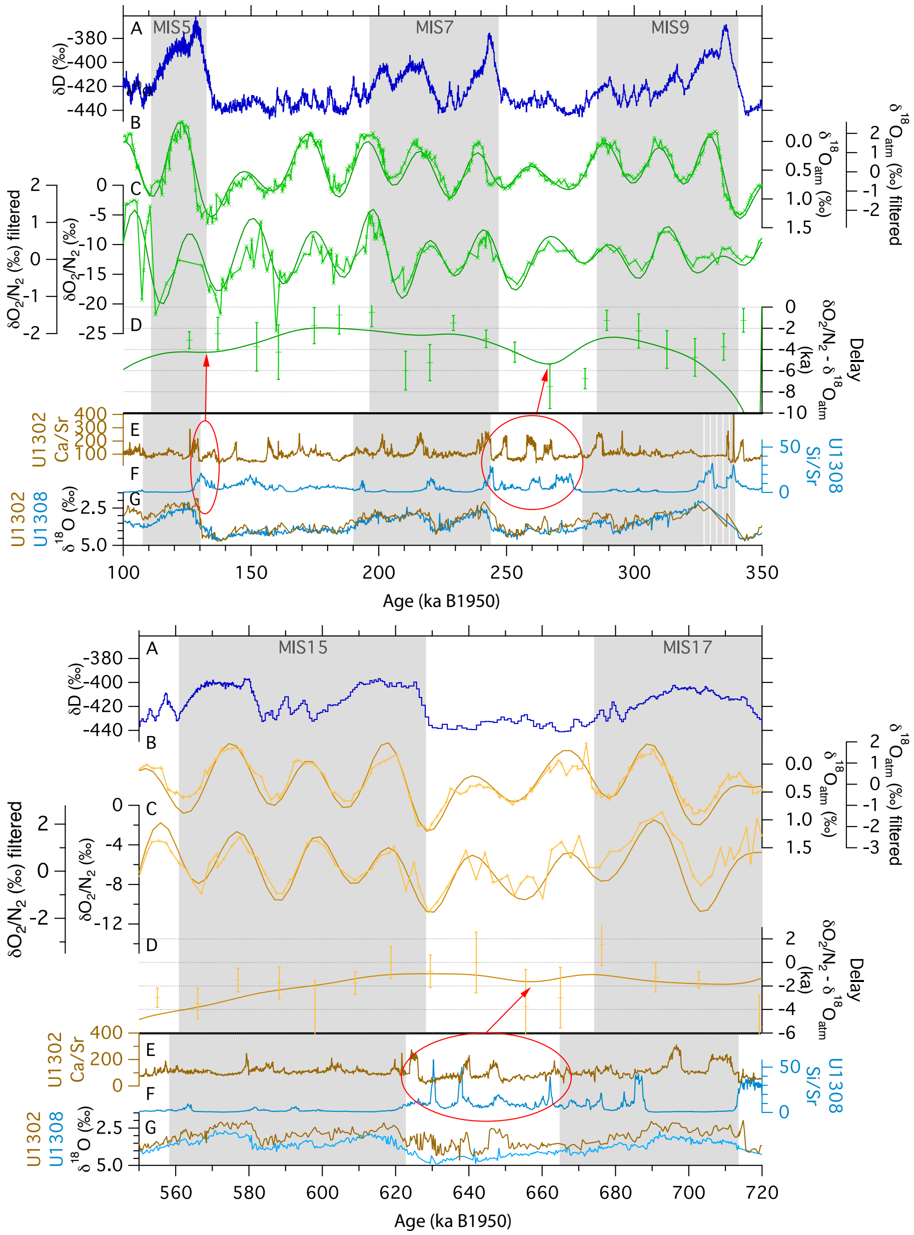

Figure 4. Evolution of the time offset between $\delta O_2/N_2$ and $\delta^{18}O_{atm}$ between 100–350 ka (top) and 550–720 ka (bottom). The Vostok data are represented in green and EDC data in yellow. The filtered data are first normalized (minus the mean and divided by the standard deviation) and then filtered between 15–100 ka using wavelet transform in Matlab. Panels A to D correspond to Vostok and EDC ice cores data on the AICC2012 chronology. A: δD of EDC, B: $\delta^{18}O_{atm}$ on reversed axis (line with markers for raw data and plain line for filtered data), C: $\delta O_2/N_2$ (line with markers for raw data and plain line for filtered data), D: time offset calculated between $\delta O_2/N_2$ and $\delta^{18}O_{atm}$using Matlab (plain curve) and manually (markers with error bars). Panels E to G present data from the U1202/03 (brown) and U1308 (light blue) presented on their respective chronology. E: Ca/Sr ratio, F: Si/Sr ratio, G: δ^{18}O planktonic for U1302/03 and δ^{18}O benthic for U1308. The grey rectangles mark the MIS intervals in both archives. The red circles and arrows show the correspondence between the ice sheets discharge events in the marine records with the maximum offset of $\delta O_2/N_2$– $\delta^{18}O_{atm}$.

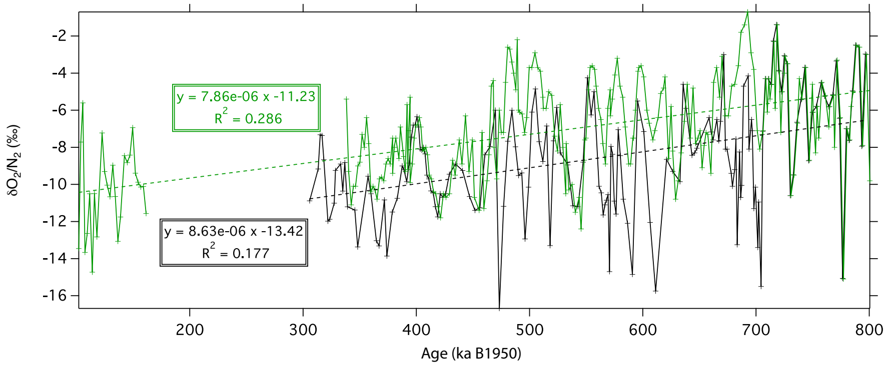

Figure A1. Comparison of the composite $\delta O_2/N_2$ record of Landais et al. (2012) (black) and the new $\delta O_2/N_2$ record measured on well–conserved ice (green). Both are presented on the AICC2012 chronology.

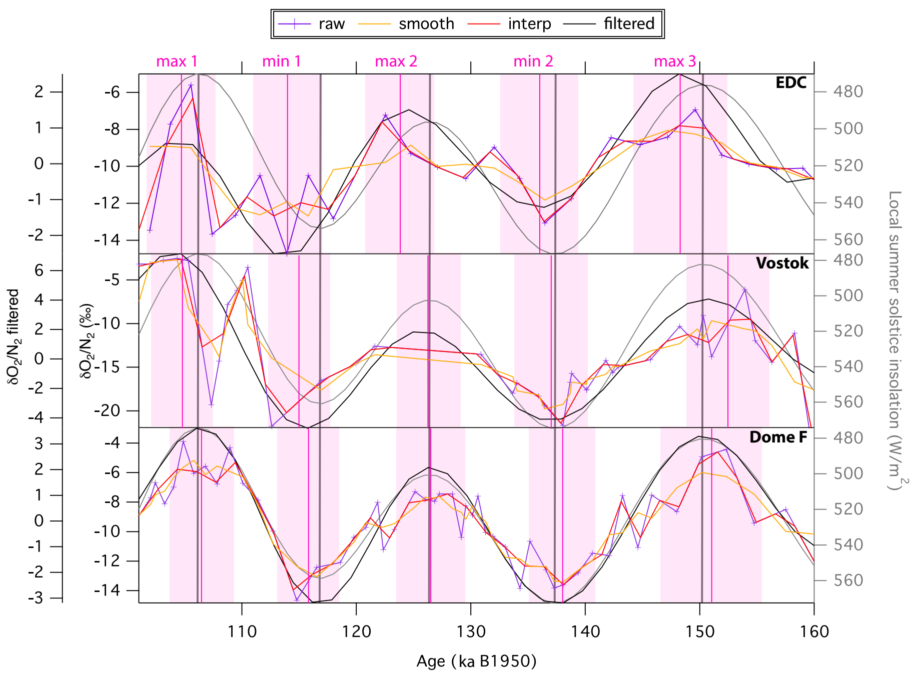

Figure B1. Determination of the uncertainty associated with $\delta O_2/N_2$ orbital tuning using different treatment of data for EDC (top), Vostok (middle) and Dome F (bottom) over MIS 5. The raw $\delta O_2/N_2$ records are presented in purple, the smoothed ones (3-points running average) are in orange, the reinterpolated curves are presented in red and the filtered records are in black. The local summer solstice insolation are represented in grey for each site. The pink vertical bars represent the mean age of minima and maxima identified, with their calculated uncertainty illustrated by the pink shaded zones. The ID of extrema indicated on top of the figure correspond to the same ID as in Table 2. The grey vertical bars show the timing of minima and maxima in the insolation curves. EDC and Vostok data are presented on AICC2012 and Dome F data on DFO-2006.

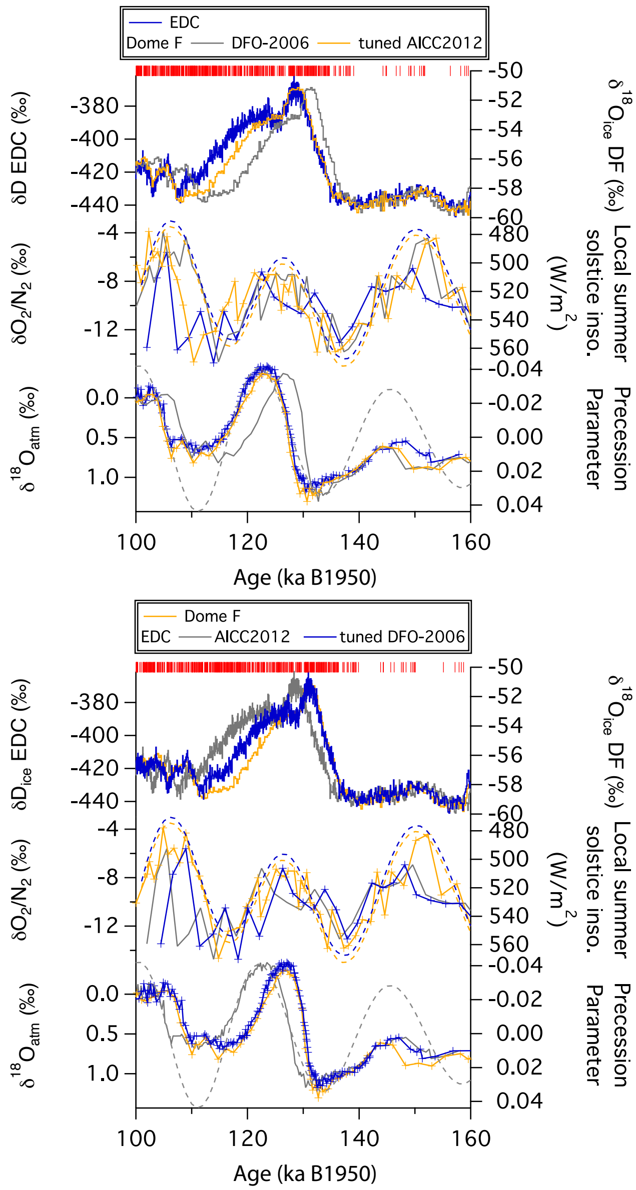

Figure C1. EDC and Dome F synchronization using volcanic matching. A: Transfert of Dome F records on AICC2012, B: transfert of EDC records on DFO-2006 using the volcanic tie points of Fujita et al. (2015). The colored curves represent EDC and Dome F records tuned together on either chronologies. The grey curves correspond to the data on their original chronology, before tuning. Top: δD record of EDC and $\delta^{18}O_{ice}$ record of Dome F. Middle: $\delta O_2/N_2$ records and local summer solstice insolation. Bottom: $\delta^{18}O_{atm}$ records and precession parameter shifted by 5 ka. The volcanic tie points are indicated by the red markers on top of the figures.